

Contents lists available at ScienceDirect

Journal of the Mechanical Behavior of Biomedical Materials

Journal of her Mechanical Behavior of Biomedical Materials

journal homepage: www.elsevier.com/locate/jmbbm



Effects of solvent osmolarity and viscosity on cartilage energy dissipation under high-frequency loading

Jin Wook Hwang ^{a,+}, Dipul Chawla ^b, Guebum Han ^{b,1}, Melih Eriten ^b, Corinne R. Henak ^{a,b,c,*}

- ^a Department of Biomedical Engineering, University of Wisconsin-Madison, Madison, WI, USA
- ^b Department of Mechanical Engineering, University of Wisconsin-Madison, Madison, WI, USA
- ^c Department of Orthopedics and Rehabilitation, University of Wisconsin-Madison, Madison, WI, USA

ARTICLE INFO

Keywords: Dynamic mechanical analyzer Cartilage Energy dissipation Osmolarity Viscosity

ABSTRACT

Articular cartilage is a spatially heterogeneous, dissipative biological hydrogel with a high fluid volume fraction. Although energy dissipation is important in the context of delaying cartilage damage, the dynamic behavior of articular cartilage equilibrated in media of varied osmolarity and viscosity is not widely understood. This study investigated the mechanical behaviors of cartilage when equilibrated to media of varying osmolarity and viscosity. Dynamic moduli and phase shift were measured at both low (1 Hz) and high (75–300 Hz) frequency, with cartilage samples compressed to varied offset strain levels. Increasing solution osmolarity and viscosity both independently resulted in larger energy dissipation and decreased dynamic modulus of cartilage at both low and high frequency. Mechanical property alterations induced by varying osmolarity are likely due to the change in permeability and fluid volume fraction within the tissue. The effects of solution viscosity are likely due to frictional interactions at the solid-fluid interface, affecting energy dissipation. These findings highlight the significance of interstitial fluid on the energy dissipation capabilities of the tissue, which can influence the onset of cartilage damage.

1. Introduction

Articular cartilage is a spatially heterogeneous, dissipative biological hydrogel composed of multiple constituents. Cartilage is roughly 20–35% extracellular matrix by wet weight (Mow and Huiskes, 2005; Chen et al., 2017). Cartilage is 10–20% collagen (mostly type II) and 10–15% proteoglycans (PGs) and glycosaminoglycans (GAGs) by wet weight (Chen et al., 2017). The constituents of the extracellular matrix govern the mechanical behavior. Tensile strength arises primarily from collagen fibers (Grushko et al., 1989; Han et al., 2011a). Compressive strength arises primarily from PGs and GAGs (Grushko et al., 1989; Han et al., 2011a). Negatively charged GAGs contribute to material behavior through charge-charge repulsion, as well as by governing fluid movement through the matrix via Donnan osmotic pressures (Zimmerman et al., 2020; Khalsa and Eisenberg, 1997; Grodzinsky et al., 1981).

Energy dissipation is an important mechanism through which materials delay the onset of damage. Because cartilage has low regenerative capacity, understanding how damage occurs, and how it can be delayed,

is an important aspect of delaying cartilage diseases. Cartilage behavior is poroviscoelastic, so it exhibits contact-length-independent viscoelastic dissipation and contact-length-dependent poroelastic dissipation (Fulcher et al., 2009; Lawless et al., 2017; Nia et al., 2011, 2013; Han et al., 2018). Fluid moving through the solid matrix results in poroelastic behavior of cartilage. Cartilage exhibits solid phase viscoelasticity, arising primarily from the intrinsic viscoelasticity of the collagen fibrils (Mak, 1986; Huang et al., 2003). We have recently shown how poroviscoelastic relaxations and dissipation influence adhesion (Han et al., 2020a), friction (Han and Eriten, 2018) and fracture initiation in cartilage (Han et al., 2019, 2021). Therefore, understanding how dissipation changes in cartilage would enable control over mechanical response, in an effort to delay damage.

By altering osmolarity and viscosity of the solvent, distinct states of the cartilage behavior can be probed. Osmotic loading has been used to identify the roles of PGs in cartilage behavior (Khalsa and Eisenberg, 1997), map the transition from tensile behavior to compressive behavior in cartilage (Chahine et al., 2004), and identify residual tissue strains

^{*} Corresponding author. Assistant Professor 3031 Mechanical Engineering Building 1513 University, Ave Madison, WI, USA. *E-mail address*: chenak@wisc.edu (C.R. Henak).

⁺ Current address: Department of Mechanical Engineering, Northwestern University, 2145 Sheridan Rd, Evanston, IL 60208.

¹ Current address: Department of Mechanical Engineering, University of Minnesota, 111 Church St SE, Minneapolis, MN.

(Narmoneva et al., 1999, 2001; Setton et al., 1998). PGs were shown to contribute to cartilage's mechanical response through both Donnan osmotic pressures and electrostatic repulsion (Zimmerman et al., 2020; Khalsa and Eisenberg, 1997). Across studies, increased osmolarity correlates with decreased stiffness as measured by equilibrium and low frequency dynamic moduli (Zimmerman et al., 2020; Khalsa and Eisenberg, 1997; Korhonen and Jurvelin, 2010a; Eisenberg and Grodzinsky, 1985). Cartilage permeability decreases with increased osmolarity (Lu et al., 2004), which would be expected to affect dissipative behavior. Although the effect of solvent viscosity on cartilage dissipative behavior has not been reported, it has been studied in the broader context of hydrogels. Theoretically, flow in a poroelastic medium is dependent on the viscosity of the solvent moving through it, as a result of visco-inertial dissipation (Carcione; Carcione and Gurevich, 2011; Long and Hui, 2016). Increased solvent viscosity has been shown to slow down crack propagation in hydrogels as a result of the increased poroelastic dissipations (Baumberger et al., 2006). Cartilage exhibits poroelastic dissipation, which stems from diffusion of interstitial fluid and is thereby dependent on solvent viscosity. Based on this prior literature, it is expected that both viscosity and osmolarity will impact cartilage dissipation.

How osmolarity and solvent viscosity affect macroscale, high-frequency dissipation and stiffness has not been characterized, yet is relevant in the context of cartilage mechanics, including adhesion, friction, and damage. Therefore, the objective of this study was to characterize the material behavior of articular cartilage as a function of solvent viscosity and osmolarity. We hypothesized that increased osmolarity and increased viscosity would result in increased energy dissipation. Porcine cartilage explants were tested in two configurations under macroscopic (4 mm diameter) contact lengths: stress relaxation with low frequency dynamic mechanical analysis (DMA) and high frequency DMA on a custom set-up (Han et al., 2020b). Samples were tested under varied concentration NaCl or with various molecular weight polyethylene glycol (PEG). Equilibrium behavior, dynamic moduli, and phase angles were reported.

2. Methods

Cartilage dynamic behavior was evaluated as a function of solvent osmolarity, solvent viscosity, and offset strain (Fig. 1). Dynamic behavior was measured in two frequency regimes: low (1 Hz) using a tabletop test machine and high (75–300 Hz) using a custom DMA (Han

et al., 2020b).

2.1. Sample preparation

Porcine patellae from ten animals were collected from a local abattoir (5–6 months old, sex unknown and assumed random). Six 4 mm diameter cylindrical samples were removed from each patella using a biopsy punch and a scalpel. Subchondral bone was removed using a microtome to create a deep surface parallel to the articular surface. Samples were kept hydrated in the relevant testing solvent with protease inhibitor (Pierce Mini Tablets, EDTA-free, Thermo Fisher, Waltham, MA) throughout testing.

A total of seven solvents were evaluated. To test the effect of solvent osmolarity on behavior, varied NaCl concentrations were made: 2 M, 0.15 M, 0.015 M, and 0.0015 M. To test the effects of solvent viscosity on behavior, phosphate-buffered saline (PBS) was augmented with varied molecular weight (MW) PEG: PBS + 10K PEG (Polyethylene Glycol MW 10000, BeanTown Chemical, Hudson, New Hampshire), PBS + 100K PEG (Polyethylene Oxide MW 100000, BeanTown Chemical, Hudson, New Hampshire). The concentration of PEG in both augmented solutions was fixed at 100 mg/ml. These solvents have viscosities of 0.88 mPa s, 3.5 mPa s, 37.2 mPa s, respectively for PBS, PBS +10K PEG, and PBS +100K PEG (Shi et al., 2011).

Six samples per patella were split into three groups with two samples per group. The groups were for testing the effect of varied NaCl concentration, PBS +10K PEG, and PBS +100K PEG. The first sample in each group was tested on dynamic loading at low frequency (1 Hz) and stress relaxation while the second group was investigated at high frequency sweep (75–300 Hz). Samples were allowed to equilibrate in the solvent for an hour prior to testing. Sample thickness was measured with calipers after equilibration, before samples were placed in testing wells (Fig. 1C). Average thicknesses were 1.66 ± 0.18 mm, 1.62 ± 0.18 mm, 1.56 ± 0.17 , and 1.51 ± 0.16 mm for $0.0015,\,0.015,\,0.15$ and 2 M NaCl, respectively. Average thicknesses were 1.54 ± 0.14 mm, 1.53 ± 0.13 mm, and 1.50 ± 0.13 mm for PBS, PBS+10k MW PEG, and PBS+100k MW PEG, respectively.

2.2. Dynamic loading at low frequency

Dynamic loading at 1 Hz was performed to understand the effect of varied NaCl concentration and solvent viscosity on dynamic modulus and phase angle. Samples were adhered to a custom testing well using

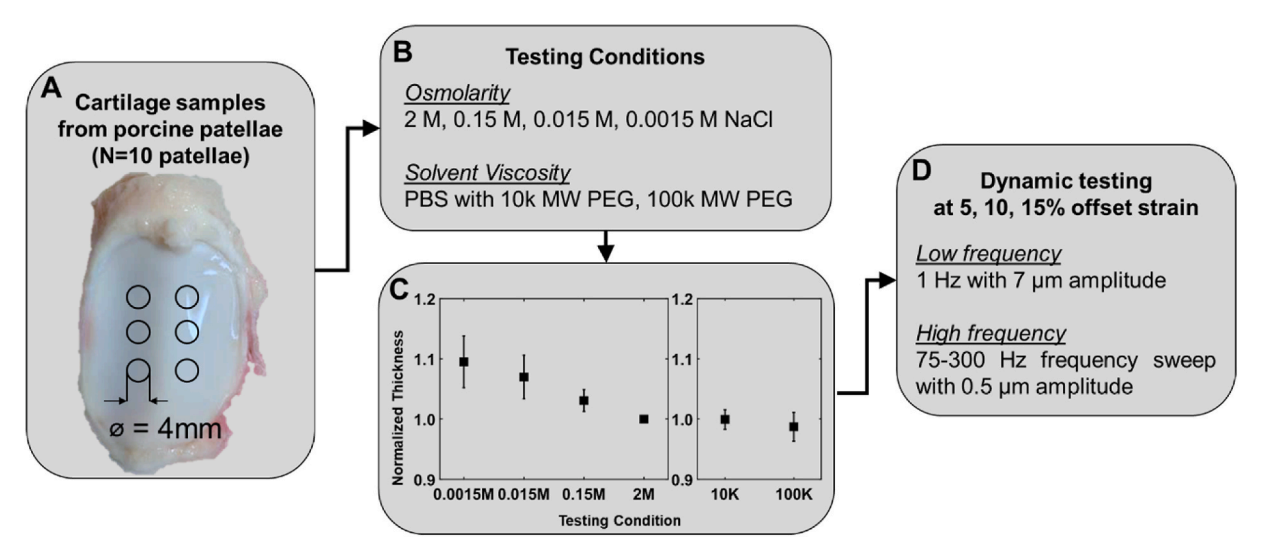


Fig. 1. Overview of study design. (A) Samples were dissected from 10 porcine patella, then (B) equilibrated in different testing solvents. (C) Normalized thickness (normalized to 2 M NaCl for osmolarity, and to PBS for viscosity) showed variation only as a function of osmolarity. (D) Dynamic testing was completed at low and high frequencies.

cyanoacrylate, with the articular surface up. Adhering the samples was necessary to keep them in place throughout testing, and resulted in a test configuration that approximates unconfined compression. Samples were compressed with a platen fully covering the sample surface and were submerged in the solvent which the samples were equilibrated to. Low frequency tests were conducted on a tabletop test machine (TA3230 AT Series III, TA Instruments, New Castle, DE) that measured load and displacement throughout the testing with 200 Hz sampling frequency. Each sample was subjected to offset strain in 5% increments, followed by 10 min of relaxation, then 50 cycles of dynamic loading with 7 μm amplitude. An additional 3 min of relaxation was given after the dynamic loads to ensure a fully relaxed sample for the next 5% increment of compression. The combination of stress-relaxation and cyclic loading was sequentially performed three times per sample to obtain dynamic response of the sample at 5%, 10% and 15% offset strains.

2.3. Dynamic loading at high frequency

A custom DMA was used to evaluate the effects of osmolarity and viscosity under high-frequency loading (75–300 Hz) (Han et al., 2020b). As with low frequency testing, samples were adhered to a custom testing well using cyanoacrylate, with the articular surface up. Samples were compressed with a platen fully covering the sample surface and was submerged in the solvent which the samples were equilibrated to. As in the low frequency experiments, dynamic responses of a sample were obtained at three different offset strains, 5%, 10%, and 15%. As in the low frequency setup, relaxation of 10 min and 3 min was allowed before and after the dynamic load, respectively. High-frequency DMA was conducted at a 0.5 µm amplitude with a frequency sweep of 75–300 Hz. The amplitude of the oscillations was controlled using a piezo actuator (PI P-250.20, PI, Auburn, MA). Load was measured throughout testing using a dynamic force sensor (PCB208C01, PI, Auburn, MA). Displacement was measured based on the double integration of acceleration measured using two accelerometers (PCB333B30, PI, Auburn, MA) located top and bottom of the stages holding the sample. The sampling frequency of the DMA at high frequency was 5 kHz.

2.4. Data analysis

For the low frequency data, equilibrium stress and relaxation time constant were calculated using the 10-min stress relaxation that preceded the dynamic loading. Equilibrium stress at a given offset strain was defined as the stress after the 10 min of relaxation. The relaxation time constant was defined as the time required to relax 90% of peak stress at compression relative to the equilibrium stress at each offset strain

Dynamic modulus and phase shift were calculated assuming linear viscoelasticity at each offset strain for both low and high frequency experiments. First Piola-Kirchhoff stress was used to quantify stress, where the measured load was divided by the reference cross-sectional area $A=\pi r^2$ where r=2 mm.

Dynamic modulus and phase shift for the low frequency range were calculated from stress-strain hysteresis loops. Hysteresis loops of the last 10 sinusoidal loads were used to eliminate the effect of stress relaxation observed at the onset of cyclic loads and obtain dynamic modulus and phase shift. The dynamic modulus E^* was obtained by fitting a line through points in the hysteresis loop corresponding to minimum and maximum points in the sinusoidal input, assuming linear viscoelastic relation $\sigma_{max} = |E^*|\varepsilon_{max}$ (Lu et al., 2004). Phase shift, δ , was obtained by calculating the lag of strain compared to the stress by fitting each component to sinusoidal functions $\sigma(t) = \sigma_0 \sin(2\pi f t)$ and $\varepsilon(t) = \varepsilon_0 \sin(2\pi f t)$ where σ_0 and ε_0 denote the corresponding amplitudes, f the frequency, and t the time (Lu et al., 2004).

The dynamic modulus and phase shift for the frequency sweep at high frequency range were calculated using frequency domain analysis. The complex dynamic stiffness $K(\omega)$ was obtained from the measured force response $F(\omega)$ and the displacements of top, $X_1(\omega)$ and bottom, $X_2(\omega)$ stages holding the sample using the following relationship:

$$K(\omega) = \frac{F(\omega)}{X_1(\omega) - X_2(\omega)} \tag{1}$$

The complex dynamic modulus $E^*(\omega)$ was calculated using the complex dynamic stiffness $K(\omega)$, sample height h at each offset strain, and reference cross section $A=\pi r^2$:

$$E^*(\omega) = \frac{K(\omega)h}{A} \tag{2}$$

The dynamic modulus and the phase shift comparable to those at low frequency were obtained by calculating the magnitude and phase of $E^*(\omega)$, respectively. All calculations were made using custom MATLAB code.

2.5. Statistical analysis

Parametric and non-parametric ANOVAs were conducted to evaluate effects of all main effects and their combinations, with the main effects being solvent molarity (NaCl), solvent viscosity (PEG), frequency, and offset strain. These effects were tested on equilibrium stress and time constant, dynamic modulus and phase shift at low frequency, and dynamic modulus and phase shift at high frequency. Only main effects were tested, with no pairwise post-hoc tests to reduce the overall number of tests. For statistical analysis, the high frequency data were binned into three levels: Low (75-150 Hz), Medium (150-225 Hz), and High (225-300 Hz). The Shapiro test was conducted along with analyzing QQ-plot and histograms to confirm the normality of the dependent variables. A two-way type-III ANOVA was performed to determine the main effect and interaction effect of molarity and offset strain level on equilibrium stress, time constant, dynamic modulus, and phase shift for 1 Hz. Similarly, a three-way ANOVA was performed to determine the main effect and interaction effect of frequency, molarity, and offset strain on dynamic modulus and phase shift for high frequency DMA data (75-300 Hz). In cases where equilibrium stress, time constant, dynamic modulus or phase shift were not normally distributed or assumptions of parametric ANOVA were not met, standard transformations were performed to attempt to achieve normality. The dynamic modulus for solvent viscosity in high frequency DMA data was transformed successfully using a log transform. If the normality was not achieved even after several transformations, non-parametric aligned rank transformation analysis of variance (ART ANOVA) was performed; only the equilibrium stress and phase angle for high frequency DMA under varied NaCl concentration could not be transformed or met the assumptions of parametric ANOVA. All statistical analysis was done using R Programming on RStudio® Version 4.0.0 (RStudio, PBC, Boston, MA). The significance value was set at $p \le 0.05$.

3. Results

3.1. Low frequency

Equilibrium stress was significantly different (p<0.05) with main effects of molarity and offset strain for both varied NaCl concentration and solvent viscosity through PEG (Fig. 2A and B, respectively). The equilibrium stress increased from 0.11 ± 0.04 MPa at 5% offset strain to 0.42 ± 0.05 MPa at 15%, 0.09 ± 0.03 MPa to 0.37 ± 0.05 MPa, 0.03 ± 0.01 MPa to 0.21 ± 0.04 MPa, and 0.02 ± 0.01 MPa to 0.12 ± 0.02 MPa at 0.0015M, 0.015M, 0.15M, and 2M concentration respectively, whereas it increased from 0.06 ± 0.02 MPa to 0.26 ± 0.11 MPa, 0.03 ± 0.01 MPa to 0.17 ± 0.03 MPa, and 0.02 ± 0.01 MPa to 0.14 ± 0.03 MPa at PBS, PBS +10K PEG, and PBS +10OK PEG concentration, respectively. Significant interaction effects (p<0.05) were observed for varied NaCl

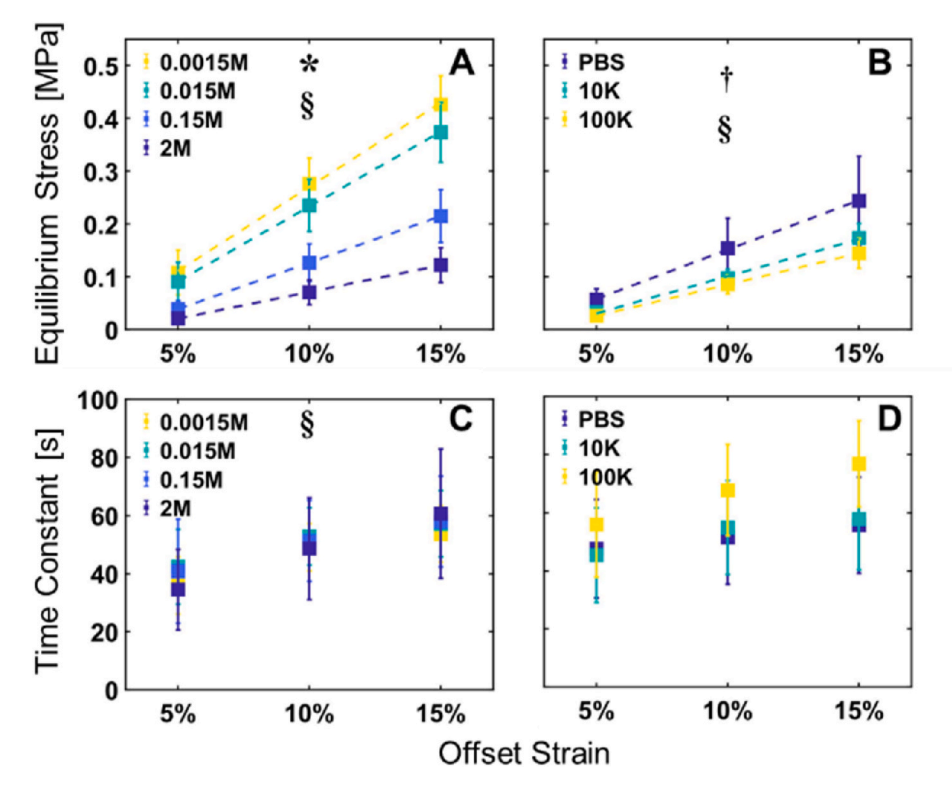


Fig. 2. Results from stress relaxation experiments. Equilibrium stress in NaCl (A) and PBS with PEG (B). Equilibrium time constants in NaCl (C) and PBS with PEG (D). * indicates a main effect of osmolarity (NaCl), † indicates a main effect of viscosity (PEG), § indicates a main effect of offset strain.

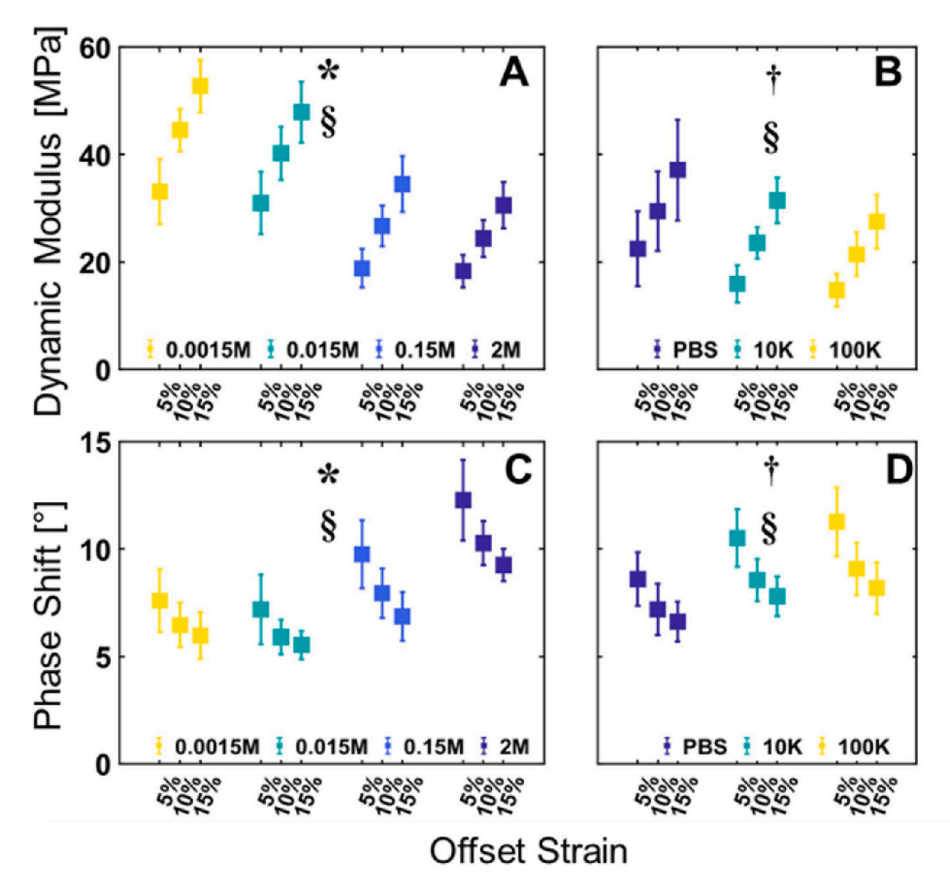


Fig. 3. Results for dynamic loading at 1 Hz. Dynamic modulus in NaCl (A) and PBS with PEG (B). Phase shift in NaCl (C) and PBS with PEG (D). Overall, dynamic modulus and phase shift have significant difference across offset strain, osmolarity, and solvent viscosity (p < 0.05). * indicates a main effect of osmolarity (NaCl), † indicates a main effect of viscosity (PEG), § indicates a main effect of offset strain.

concentration whereas no interactions were significant (p>0.05) in case of viscosity induced by PEG. Time constant was significant (p<0.05) with main effects of offset strain but not with molarity of the NaCl solution (Fig. 2C). It varied from 35.91 ± 9.38 s at 5% offset strain to 53.65 ± 9.17 s at 15%, 42.38 ± 12.24 s to 57.18 ± 10.81 s, 40.84 ± 16.96 s to 57.95 ± 14.81 s, and 34.48 ± 13.14 s to 60.62 ± 21.07 s at 0.0015M, 0.015M, 0.15M, and 2M concentration, respectively. In case of different PEG solutions, time constant did not have significant change (p>0.05) with solvent viscosity or offset strain (Fig. 2D). The time constant had a similar trend for PEG solutions like NaCl concentration, it increased 49.29 ± 17.84 s to 57.39 ± 19.32 s, 45.38 ± 15.43 s to 57.76 ± 16.57 s, and 55.95 ± 17.164 s to 76.82 ± 13.98 s at PBS, PBS +10K PEG, and PBS +100K PEG concentration, respectively. No interaction effect between the main effects on time constant were observed for both NaCl and PEG solution cases.

Dynamic modulus and phase shift were significantly affected by the offset strain and solvent used for tests ((p < 0.05) Fig. 3). No significant (p > 0.05) interaction effect was observed in dynamic modulus or phase shift for both NaCl and PEG solutions. For varied NaCl concentration, dynamic modulus ranged from 33.12 \pm 5.72 MPa at 5% offset strain to 52.74 \pm 4.64 MPa at 15% offset strain, 30.97 \pm 5.46 to 47.89 \pm 5.39 MPa, 18.81 \pm 3.39 to 34.48 \pm 4.90 MPa, and 18.28 \pm 2.86 to 30.56 \pm 4.10 MPa (Fig. 3A); whereas phase shift varied from 7.59 \pm 1.38 to 5.96 $\pm~1.02^{\circ},~7.18~\pm~1.53~$ to $5.53~\pm~0.61^{\circ},~9.74~\pm~1.55~$ to $6.85~\pm~1.07^{\circ},~$ and 12.26 ± 1.77 to $9.25 \pm 0.71^{\circ}$ (Fig. 3B) at 0.0015M, 0.015M, 0.15M, and 2M concentration, respectively. Similar trends in modulus and phase shift were observed when the solvent viscosity was changed by addition of different molecular weight of PEG. Dynamic modulus approximately doubled from 5% offset strain to 15% offset strain for every PEG concentration. It varied from 24.17 \pm 9.01 MPa at 5% offset strain to 39.80 \pm 11.50 MPa at 15% offset strain, 15.93 \pm 3.27 to 31.47 \pm 4.03 MPa, and 14.76 \pm 2.85 to 27.51 \pm 4.78 MPa (Fig. 3C); whereas phase shift varies from 8.39 ± 1.49 to $6.39 \pm 0.98^{\circ},\, 10.51 \pm 1.26$ to $7.79 \pm 0.88^{\circ},\,$ and 11.26 \pm 1.51 to 8.17 \pm 1.13° (Fig. 3D) at PBS, PBS + 10K PEG, and PBS + 100K PEG concentration, respectively.

3.2. High frequency

Dynamic modulus and phase shift were significantly affected by offset strain, frequency, and solvent for tests conducted in both NaCl and PEG (Figs. 4 and 5). Overall, the main effects of frequency, molarity, offset strain and two-way interaction of frequency-molarity and molarity-offset strain on dynamic modulus were significant (p < 0.05). No significant two-way interaction of frequency-offset strain or three-way interaction of frequency-molarity-offset strain were observed on dynamic modulus in case of NaCl varied concentrations (Fig. 4A–C). However, all individual factors, their two-way interaction, and three-way interaction had a significant (p < 0.05) effect on phase shift (Fig. 4D–F). Overall, all individual factors, their two-way interaction, and three-way interaction had significant (p < 0.05) effect on dynamic modulus (Fig. 5A–C) and phase shift in case of PEG solvent viscosity variation (Fig. 5D–F).

Dynamic modulus and phase shift showed an increasing trend with frequency under varied NaCl concentration (Fig. 4). At the lowest frequency (75 Hz), the dynamic modulus varied from 48.97 \pm 15.94 MPa at 5% offset strain to 58.54 \pm 18.94 MPa at 15% offset strain, 41.12 \pm 10.41 to 50.30 ± 6.80 MPa, 31.12 ± 10.21 to 39.88 ± 12.66 MPa, and 35.16 ± 6.70 to 42.70 ± 7.28 MPa; whereas phase shift varied from 5.18 $\pm~0.35$ to 4.58 $\pm~0.33^{\circ},\,5.93\pm1.02$ to 5.02 $\pm~0.54^{\circ},\,8.45\pm0.61$ to 7.27 \pm 0.53°, and 9.73 \pm 0.72 to 8.39 \pm 0.43° at 0.0015M, 0.015M, 0.15M, and 2M concentration, respectively. At the highest frequency (300 Hz), the dynamic modulus varied from 52.82 \pm 17.33 MPa at 5% offset strain to 62.04 \pm 20.13 MPa at 15% offset strain, 45.06 \pm 11.27 to 54.07 \pm 7.06 MPa, 35.55 \pm 11.84 to 44.27 \pm 14.21 MPa, and 40.17 \pm 7.51 to 47.49 ± 7.84 MPa; whereas phase shift varied from 6.52 ± 0.52 to 5.98 $\pm~0.46^{\circ}$, 7.15 ± 1.12 to $6.34\pm0.53^{\circ}$, 10.48 ± 0.73 to $9.12\pm0.59^{\circ}$, and 11.02 ± 0.71 to $9.89 \pm 0.55^{\circ}$ at 0.0015M, 0.015M, 0.15M, and 2Mconcentration, respectively.

Solvent viscosity variation due to PEG concentration surrounding the cartilage samples showed an increasing trend with frequency (Fig. 5). At lowest frequency, the dynamic modulus varied from 32.17 \pm 11.68 MPa at 5% offset strain to 38.64 \pm 13.73 MPa at 15% offset strain, 24.67 \pm 2.57 to 34.11 \pm 4.67 MPa, and 26.39 \pm 6.17 to 36.52 \pm 8.56 MPa,

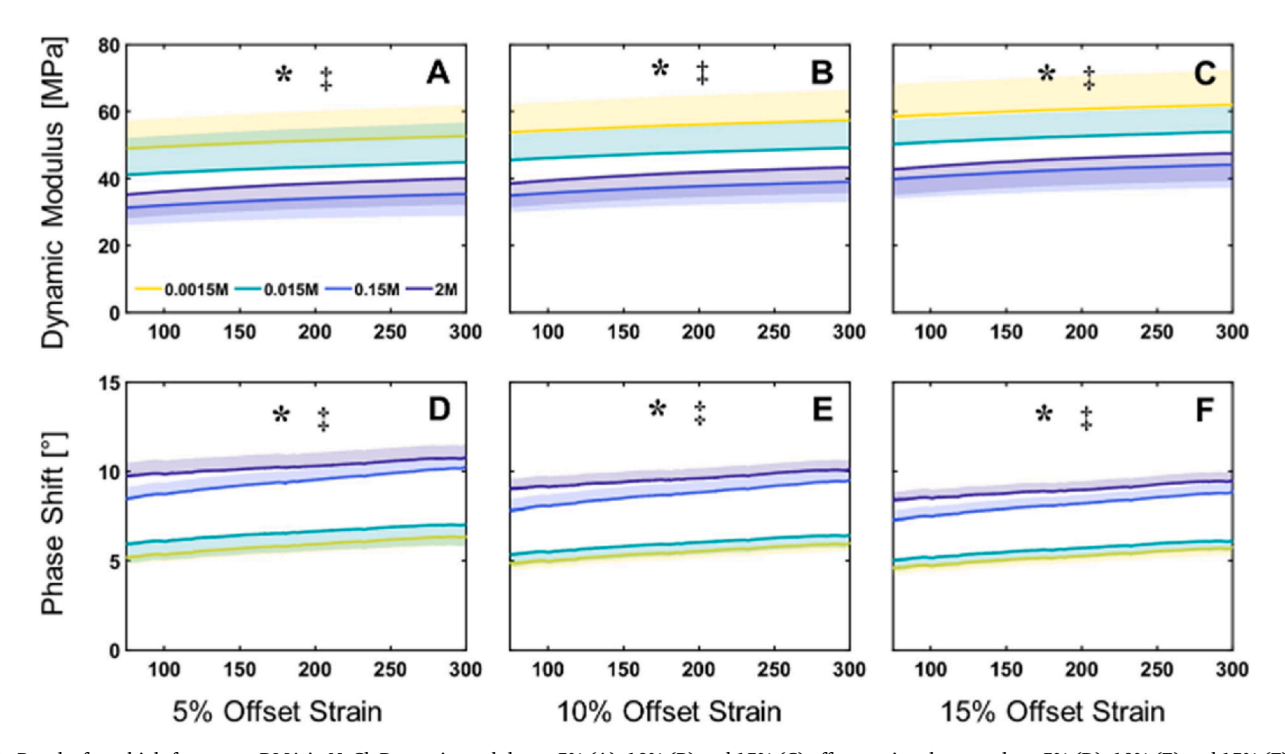


Fig. 4. Results from high-frequency DMA in NaCl. Dynamic modulus at 5% (A), 10% (B) and 15% (C) offset strain; phase angle at 5% (D), 10% (E) and 15% (F) offset strain. * indicates a main effect of osmolarity (NaCl), ‡ indicates a main effect of frequency. Offset strain (between columns) was a significant main effect.

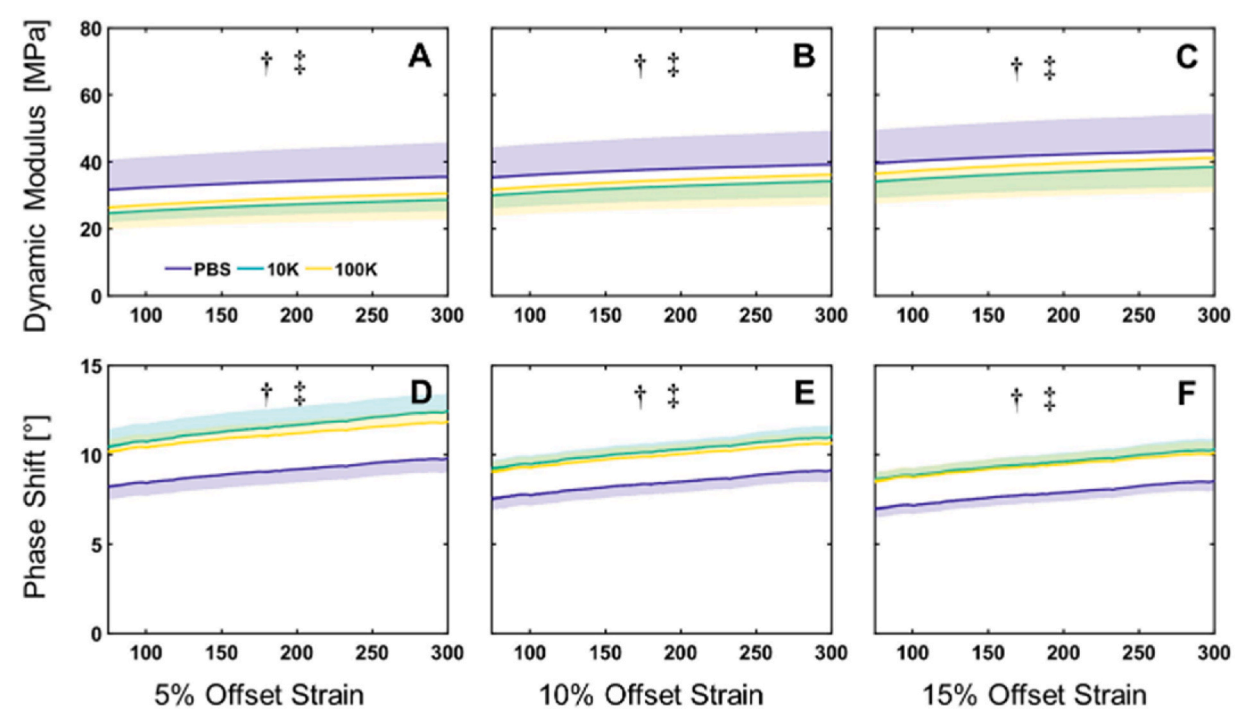


Fig. 5. Results from high-frequency DMA in PBS with PEG. Dynamic modulus at 5% (A), 10% (B) and 15% (C) offset strain; phase angle at 5% (D), 10% (E) and 15% (F) offset strain. † indicates a main effect of viscosity (PEG), ‡ indicates a main effect of frequency. Offset strain (between columns) was a significant main effect.

whereas phase shift varied from 8.02 ± 0.83 to $6.79\pm0.54^\circ$, 10.43 ± 0.92 to $8.60\pm0.31^\circ$, and 10.14 ± 0.66 to $8.50\pm0.49^\circ$ at PBS, PBS +10K PEG, and PBS +100K PEG concentration, respectively. At the highest frequency, the dynamic modulus varied from 35.97 ± 13.11 MPa at 5% offset strain to 41.77 ± 14.33 MPa at 15% offset strain, 28.88 ± 3.28 to 38.66 ± 5.74 MPa, and 30.82 ± 7.51 to 41.41 ± 9.87 MPa; whereas phase shift varied from 10.01 ± 0.71 to $8.88\pm0.59^\circ$, 12.65 ± 0.98 to $10.57\pm0.76^\circ$, and 12.01 ± 0.68 to $10.33\pm0.71^\circ$ at PBS, PBS +10K PEG, and PBS +100K PEG concentration, respectively.

4. Discussion

The objective of this study was to characterize the material behavior of articular cartilage as a function of solvent viscosity and osmolarity. Both study hypotheses were confirmed: increased osmolarity increased energy dissipation, and increased viscosity increased energy dissipation. This was confirmed by evaluating the phase shift, the tangent of which yields loss tangent $tan\delta$, a quantity associated with the ratio of dissipated energy to the stored energy under oscillatory loading (Lu et al., 2004). Thus, the phase shift was used as a measure of energy dissipation in the following discussion to gain insight into the rationale behind altered cartilage behaviors equilibrated to solvents of varying osmolarity and viscosity. Many of the results can be interpreted based on the influence of solvent viscosity, frequency, porosity, permeability, and modulus; which can be related by interpreting cartilage as a poroelastic medium and uniaxial loading inducing diffusion in transverse directions and delivering phase shift approximately as (Dawson et al., 2008a) (derivation in Supplementary Data):

$$\delta \approx \frac{\mu R^2 \omega}{8\Phi kE} \tag{3}$$

where μ is the dynamic viscosity of the fluid, R is the sample radius, ω is the loading frequency, Φ is the sample porosity, k is the permeability and E is the sample modulus. This equation assumes that the radius is larger than the height (Dawson et al., 2008a). In line with this expression, across solvents, an increasing trend in phase angle was observed with increasing loading frequency, while phase angle and dynamic

modulus were inversely related (Figs. 3–5). Within the solvents of different viscosities, the phase angle increased with viscosity. The relationship between phase angle and porosity and permeability becomes more complicated, as porosity and permeability are both dependent on volumetric strain in cartilage (Ateshian et al., 1997; Holmes and Mow, 1990; Lai et al., 1981), yet, they are in competition in their potential effects on the phase angle. Additional effects result from the viscoelastic contribution of the collagen fibers, and of electrostatic charge repulsion.

The effects of osmolarity are likely due to alterations in porosity. permeability, collagen reference configuration, and electrostatic charge repulsion. Increasing osmolarity affects the swollen state of the tissue. At physiological osmolarity, approximated by 0.15 M NaCl in this study, collagen fibers are under tension (Eisenberg and Grodzinsky, 1985; Han et al., 2011b; Mow et al., 1992; Urban et al., 1979; Soriano-garcia, 1976). As the osmolarity of the solvent increases, the thickness decreases, causing decreased collagen tension and increased electrostatic repulsion between negatively charged PGs (Fig. 1C) (Grodzinsky et al., 1981; Mow et al., 1999; Wachtel and Maroudas, 1998; Myers et al., 1984). By decreasing the collagen tension, the fibrils would be moved to a regime where they can dissipate more energy through viscoelastic relaxations (Mak, 1986; Huang et al., 2003; Puxkandl et al., 2002; Bonifasi-Lista et al., 2005). Cartilage permeability decreases with increased osmolarity (Lu et al., 2004). According to the approximate expression for the phase shift, this would also mean increase in poroelasticity-related energy dissipation. This was observed experimentally (see Fig. 3C and D). Equilibrium stress and dynamic modulus decreased with increased osmolarity, consistent with previous literature (Zimmerman et al., 2020; Korhonen and Jurvelin, 2010b). This decrease is likely due to the shrinking of the collagen fibers, which are not compensated for by electrostatic repulsion.

The effects of PEG solutions are driven predominantly by their viscosity. This is consistent with the basis of dissipation in poroelastic media (Carcione; Carcione and Gurevich, 2011; Long and Hui, 2016; Dawson et al., 2008a). Furthermore, a previous study of PEG solution on a quartz crystal resonator confirms the MW dependence of PEG solution's viscosity at fluid-solid boundary layer (Wang et al., 2009).

Specifically, a monotonic increase in dissipation factor of PEG solution was observed with the increase in PEG MW at a concentration higher than 100 mg/ml. This matches with the higher energy dissipation observed in the samples equilibrated to PBS+10K PEG and PBS+100K PEG as compared to PBS. The decreased dynamic modulus in high MW PEG solution is analogous to typical behaviors of crosslinked PEG hydrogels. Varying the MW of PEG is often utilized to tune hydrogel's properties, where higher MW PEG is used to yield lower Young's modulus. In addition to viscosity, the differences in modulus could arise from osmotic pressures. Although not charged, the PEG solutions will create osmotic pressure (Chang and Kaplan, 1977). For the two PEG solutions used here, the difference in osmotic pressure is roughly 0.03 MPa, which is consistent with the differences measured between PEG concentrations in equilibrium stress, but smaller than the differences measured in dynamic modulus. The lack of statistical difference in most measures between the two different PEGs may result from the difficulty of the larger PEG diffusing into cartilage, as larger molecules diffuse less easily in cartilage (DiDomenico et al., 2017; DiDomenico and Bonassar, 2018). Thus, while the effects of PEG were significant in this study, the direct equilibration of PEG solution is a challenging way of perturbing cartilage behavior and may not be the most fruitful method for further study.

Offset strain and excitation frequency affected modulus and dissipation measures. Phase shift decreased with increased offset strain, while modulus increased with increased offset strain. With increasing strain, the effective pore size decreases, which would affect both permeability and porosity. At the same time, the modulus would be expected to increase because of the compaction of the sample. The dynamic modulus and phase shift increased with frequency (75–300 Hz), consistent with previous studies (Mountcastle et al., 2019); however, our study focused on a higher frequency range than previously evaluated.

This study includes limitations that are worth considering. Our study evaluated the dynamic response, phase shift, and equilibrium response at successive compression offset strain similar to a previous study (Nguyen and Levenston, 2012). Although the testing conditions did not directly mimic in vivo conditions, the alterations in solvent osmolarity and viscosity, the range of frequencies, and the range of offset strain can be compared to in vivo cases. Solvent osmolarity ranges from 350 to 450 mOsm in vivo in healthy joints, but can drop to 280 mOsm in disease states, and synovial fluid viscosity is ~5-150 mPa s, depending on the shear rate (Sampat et al., 2013; Shanfield et al., 1988; Martin-Alarcon and Schmidt, 2016). Typical physiological frequency while walking, running, and sprinting is approximated to be within a range of 0.5–10 Hz (Tamer, 2013), although higher rate loading occurs during foot strike (Lieberman et al., 2010). Quasistatic strains measured in vivo using magnetic resonance imaging suggests offset strains of 2-10% (Cher et al., 2016; Coleman et al., 2013; Liu et al., 2017; Owusu-Akyaw et al., 2017; Sutter et al., 2015, 2019; Collins et al., 2018; Chan et al., 2016), while dynamic strains measured using computed tomography or biplane fluoroscopy are 17-29% (Halonen et al., 2014; Carter et al., 2015; Bischof et al., 2010). Thus, despite the limitation of not directly matching all in vivo conditions, our results can be compared to in vivo ranges and our study provides insight into mechanisms of energy dissipation in cartilage.

In conclusion, this study showed dependence of dynamic cartilage properties on solvent osmolarity and viscosity. Manipulating solvent osmolarity and viscosity led to swelling of the cartilage tissue and altered energy dissipation, further inducing changes in mechanical responses. These findings empirically demonstrate the combined roles of the matrix configuration, which influences porosity, permeability, and collagen fiber configuration; as well as the role of solvent viscosity in shifting cartilage matrix behavior. Tuning energy dissipation has the potential to influence the onset of damage in cartilage. Furthermore, such mechanical behaviors are a potential reference for creating cartilage-inspired soft materials (e.g. Han et al., 2020c).

The use of osmolarity and viscosity to evaluate changes in dissipative properties in this paper provide important foundational data. One context in which energy dissipation is important in cartilage function and in disease is failure. Increased energy dissipation can delay fracture nucleation; we have demonstrated this using depletion of proteoglycans to alter dissipation at intermediate loading rates (Han et al., 2021). Understanding the effects of osmolarity and viscosity on energy dissipation serves as the foundation for future work understanding the effects of osmolarity and viscosity on fracture nucleation.

Author statement

JH: data collection, formal analysis, visualization, writing – original draft, writing – review & editing; DC: formal analysis, visualization, writing – original draft, writing – review & editing; GH: conceptualization, methodology, data collection, writing – original draft, writing – review & editing; ME: conceptualization, funding acquisition, resources, supervision, visualization, writing – original draft, writing – review & editing; CRH: conceptualization, funding acquisition, resources, supervision, visualization, writing – original draft, writing – review & editing.

Declaration of competing interest

The authors declare that they have no known competing financial interests or personal relationships that could have appeared to influence the work reported in this paper.

Acknowledgments

Funding from the National Science Foundation (CMMI-DCSD-1662456) is gratefully acknowledged. Assistance with statistics from Shannon K. Walsh is gratefully acknowledged.

Appendix A. Supplementary data

Supplementary data to this article can be found online at https://doi.org/10.1016/j.jmbbm.2021.105014.

References

- Ateshian, G.A., Warden, W.H., Kim, J.J., Grelsamer, R.P., Mow, V.C., 1997. Finite deformation biphasic material properties of bovine articular cartilage from confined compression experiments. J. Biomech. 30 (11–12), 1157–1164.
- Baumberger, T., Caroli, C., Martina, D., 2006. Solvent control of crack dynamics in a reversible hydrogel. Nat. Mater. 5 (7), 552–555.
- Bischof, J.E., Spritzer, C.E., Caputo, A.M., Easley, M.E., DeOrio, J.K., Nunley, J.A., DeFrate, L.E., 2010. In vivo cartilage contact strains in patients with lateral ankle instability. J. Biomech. 43 (13), 2561–2566.
- Bonifasi-Lista, C., Lake, S.P., Small, M.S., Weiss, J.A., 2005. Viscoelastic properties of the human medial collateral ligament under longitudinal, transverse and shear loading. J. Orthop. Res. 23 (1), 67–76.
- Carcione, J.M., Gurevich, B., 2011. Differential form and numerical implementation of biot's poroelasticity equations with squirt dissipation. Geophysics 76 (6), N55–N64.
- Carter, T.E., Taylor, K.A., Spritzer, C.E., Utturkar, G.M., Taylor, D.C., Moorman, C.T., Garrett, W.E., Guilak, F., McNulty, A.L., DeFrate, L.E., 2015. In vivo cartilage strain increases following medial meniscal tear and correlates with synovial fluid matrix metalloproteinase activity. J. Biomech. 48 (8), 1461–1468.
- Chahine, N.O., Wang, C.C.-B., Hung, C.T., Ateshian, G.A., 2004. Anisotropic strain-dependent material properties of bovine articular cartilage in the transitional range from tension to compression. J. Biomech. 37 (8).
- Chan, D.D., Cai, L., Butz, K.D., Trippel, S.B., Nauman, E.A., Neu, C.P., 2016. In vivo articular cartilage deformation: noninvasive quantification of intratissue strain during joint contact in the human knee. Sci. Rep. 6 (January), 1–14.
- Chang, R., Kaplan, L.J., 1977. The donnan equilibrium and osmotic pressure. J. Chem. Educ. 54 (4), 218.
- Chen, S., Fu, P., Wu, H., Pei, M., 2017. Meniscus, Articular Cartilage, and Nucleus Pulposus: A Comparative Review of Cartilage-like Tissues in Anatomy, Development, and Function.
- Cher, W.L., Utturkar, G.M., Spritzer, C.E., Nunley, J.A., DeFrate, L.E., Collins, A.T., 2016. An analysis of changes in in vivo cartilage thickness of the healthy ankle following dynamic activity. J. Biomech. 49 (13), 3026–3030.
- Coleman, J.L., Widmyer, M.R., Leddy, H.A., Utturkar, G.M., Spritzer, C.E., Moorman, C. T., Guilak, F., DeFrate, L.E., 2013. Diurnal variations in articular cartilage thickness and strain in the human knee. J. Biomech. 46 (3), 541–547.

- Collins, A.T., Kulvaranon, M.L., Cutcliffe, H.C., Utturkar, G.M., Smith, W.A.R., Spritzer, C.E., Guilak, F., Defrate, L.E., 2018. Obesity alters the in vivo mechanical response and biochemical properties of cartilage as measured by MRI. Arthritis Res. Ther. 20 (1), 1-9.
- Dawson, M.A., McKinley, G.H., Gibson, L.J., 2008. The dynamic compressive response of open-cell foam impregnated with a Newtonian fluid. J. Appl. Mech. Trans. ASME 75 (4), 0410151–04101511.
- DiDomenico, C.D., Bonassar, L.J., 2018. How can 50 Years of solute transport data in articular cartilage inform the design of arthritis therapeutics? Osteoarthritis Cartilage 26 (11), 1438–1446.
- DiDomenico, C.D., Goodearl, A., Yarilina, A., Sun, V., Mitra, S., Sterman, A.S., Bonassar, L.J., 2017. The effect of antibody size and mechanical loading on solute diffusion through the articular surface of cartilage. J. Biomech. Eng. 139 (9), 91005.
- Eisenberg, S.R., Grodzinsky, A.J., 1985. Swelling of articular cartilage and other connective tissues: electromechanochemical forces. J. Orthop. Res. 3 (2), 148–159.
- Fulcher, G.R., Hukins, D.W.L., Shepherd, D.E.T., 2009. Viscoelastic properties of bovine articular cartilage attached to subchondral bone at high frequencies. BMC Muscoskel. Disord. 10 (1), 1–7.
- Grodzinsky, A.J., Roth, V., Myers, E., Grossman, W.D., Mow, V.C., 1981. The significance of electromechanical and osmotic forces in the nonequilibrium swelling behavior of articular cartilage in tension. J. Biomech. Eng. 103 (4), 221.
- Grushko, G., Schneiderman, R., Maroudas, A., 1989. "Some biochemical and biophysical parameters for the study of the pathogenesis of osteoarthritis: a comparison between the processes of ageing and degeneration in human hip cartilage," connect. Tissue Res. 19 (2–4), 149–176.
- Halonen, K.S., Mononen, M.E., Jurvelin, J.S., Töyräs, J., Salo, J., Korhonen, R.K., 2014. Deformation of articular cartilage during static loading of a knee joint - experimental and finite element analysis. J. Biomech. 47 (10), 2467–2474.
- Han, G., Eriten, M., 2018. Effect of relaxation-dependent adhesion on pre-sliding response of cartilage. R. Soc. Open Sci. 5 (5).
- Han, E., Chen, S.S., Klisch, S.M., Sah, R.L., 2011a. Contribution of proteoglycan osmotic swelling pressure to the compressive properties of articular cartilage. Biophys. J. 101 (4), 916–924.
- Han, E., Chen, S.S., Klisch, S.M., Sah, R.L., 2011b. Contribution of proteoglycan osmotic swelling pressure to the compressive properties of articular cartilage. Biophys. J. 101 (4), 916–924.
- Han, G., Hess, C., Eriten, M., Henak, C.R., 2018. Uncoupled poroelastic and intrinsic viscoelastic dissipation in cartilage. J. Mech. Behav. Biomed. Mater. 84 (February), 28–34.
- Han, G., Eriten, M., Henak, C.R., 2019. Rate-dependent crack nucleation in cartilage under microindentation. J. Mech. Behav. Biomed. Mater 96, 186–192.
- Han, G., Eriten, M., Henak, C.R., 2020a. Rate-dependent adhesion of cartilage and its relation to relaxation mechanisms. J. Mech. Behav. Biomed. Mater. 102.
- Han, G., Boz, U., Eriten, M., Henak, C.R., 2020b. Glycosaminoglycan depletion increases energy dissipation in articular cartilage under high-frequency loading. J. Mech. Behav. Biomed. Mater. 110 (May), 103876.
- Han, G., Boz, U., Liu, L., Henak, C.R., Eriten, M., 2020c. Indenter–foam dampers inspired by cartilage: dynamic mechanical analyses and design. J. Vib. Acoust. 142 (5), 1–9.
- Han, G., Chowdhury, U., Eriten, M., Henak, C.R., 2021. Relaxation capacity of cartilage is a critical factor in rate- and integrity-dependent fracture. Sci. Rep. 11 (1), 1–12.
- Holmes, M.H., Mow, V.C., 1990. The nonlinear characteristics of soft gels and hydrated connective tissus in ultrafiltration. J. Biomech. 23 (11), 1145–1156.
- Huang, C.-Y., Soltz, M.A., Kopacz, M., Mow, V.C., Ateshian, G.A., 2003. Experimental verification of the roles of intrinsic matrix viscoelasticity and tension-compression nonlinearity in the biphasic response of cartilage. J. Biomech. Eng. 125 (1), 84–93.
- Khalsa, P.S., Eisenberg, S.R., 1997. Compressive behavior of articular cartilage is not completely explained by proteoglycan osmotic pressure. J. Biomech. 30 (6), 589–594
- Korhonen, R.K., Jurvelin, J.S., 2010a. Compressive and tensile properties of articular cartilage in axial loading are modulated differently by osmotic environment. Med. Eng. Phys. 32 (2), 155–160.
- Korhonen, R.K., Jurvelin, J.S., 2010b. Compressive and tensile properties of articular cartilage in axial loading are modulated differently by osmotic environment. Med. Eng. Phys. 32 (2), 155–160.
- Lai, W.M., Mow, V.C., Roth, V., 1981. Effects of nonlinear strain-dependent permeability and rate of compression on the stress behavior of articular cartilage. J. Biomech. Eng. 103 (2), 61–66.
- Lawless, B.M., Sadeghi, H., Temple, D.K., Dhaliwal, H., Espino, D.M., Hukins, D.W.L., 2017. Viscoelasticity of articular cartilage: analysing the effect of induced stress and the restraint of bone in a dynamic environment. J. Mech. Behav. Biomed. Mater. 75 (July), 293–301.
- Lieberman, D.E., Venkadesan, M., Werbel, W.A., Daoud, A.I., Dandrea, S., Davis, I.S., Mangeni, R.O., Pitsiladis, Y., 2010. Foot strike patterns and collision forces in habitually barefoot versus shod runners. Nature 463 (7280), 531–535.
- Liu, B., Lad, N.K., Collins, A.T., Ganapathy, P.K., Utturkar, G.M., McNulty, A.L., Spritzer, C.E., Moorman, C.T., Sutter, E.G., Garrett, W.E., DeFrate, L.E., 2017. In vivo tibial cartilage strains in regions of cartilage-to-cartilage contact and cartilage-tomeniscus contact in response to walking. Am. J. Sports Med. 45 (12), 2817–2823.
- Long, R., Hui, C.Y., 2016. Fracture toughness of hydrogels: measurement and interpretation. Soft Matter 12 (39), 8069–8086.

- Lu, X.L., Sun, D.D.N., Guo, X.E., Chen, F.H., Lai, W.M., Mow, V.C., 2004. Indentation determined mechanoelectrochemical properties and fixed charge density of articular cartilage. Ann. Biomed. Eng. 32 (3), 370–379.
- Mak, A.F., 1986. The apparent viscoelastic behaviour of articular cartilage the contributions from the intrinsic matrix viscoplasticity and interstitial fluid flows. J. Biomech. Eng. 108, 123–130. (Accessed May 1986).
- Martin-Alarcon, L., Schmidt, T.A., 2016. Rheological effects of macromolecular interactions in synovial fluid. Biorheology 53 (2), 49–67.
- Mountcastle, S.E., Allen, P., Mellors, B.O.L., Lawless, B.M., Cooke, M.E., Lavecchia, C.E., Fell, N.L.A., Espino, D.M., Jones, S.W., Cox, S.C., 2019. Dynamic viscoelastic characterisation of human osteochondral tissue: understanding the effect of the cartilage-bone interface. BMC Muscoskel. Disord. 20 (1), 1–13.
- Mow, V.C., Huiskes, R., 2005. Basic Orthopaedic Biomechanics and Mechano-Biology. Lippincott Williams & Wilkins, Philadelphia, PA.
- Mow, V.C., Ratcliffe, A., Robin Poole, A., 1992. Cartilage and diarthrodial joints as paradigms for hierarchical materials and structures. Biomaterials 13 (2), 67–97.
- Mow, V.C., Wang, C.C., Hung, C.T., 1999. The extracellular matrix, interstitial fluid and ions as a mechanical signal transducer in articular cartilage. Osteoarthritis Cartilage 7 (1), 41–58.
- Myers, E.R., Lai, W.M., Mow, V.C., 1984. A continuum theory and an experiment for the ion–induced swelling behavior of articular cartilage. J. Biomech. Eng. 106 (2), 151–158.
- Narmoneva, D.A., Wang, J.Y., Setton, L.A., 1999. Nonuniform swelling-induced residual strains in articular cartilage. J. Biomech. 32 (4), 401–408.
- Narmoneva, D.A., Wang, J.Y., Setton, L.A., 2001. A noncontacting method for material property determination for articular cartilage from osmotic loading. Biophys. J. 81 (6), 3066–3076.
- Nguyen, A.M., Levenston, M.E., 2012. Comparison of osmotic swelling influences on meniscal fibrocartilage and articular cartilage tissue mechanics in compression and shear. J. Orthop. Res. 30 (1), 95–102.
- Nia, H.T., Han, L., Li, Y., Ortiz, C., Grodzinsky, A., 2011. Poroelasticity of cartilage at the nanoscale. Biophys. J. 101 (9), 2304–2313.
- Nia, H.T., Bozchalooi, I.S., Li, Y., Han, L., Hung, H.H., Frank, E., Youcef-Toumi, K., Ortiz, C., Grodzinsky, A., 2013. High-bandwidth AFM-based rheology reveals that cartilage is most sensitive to high loading rates at early stages of impairment. Biophys. J. 104 (7), 1529–1537.
- Owusu-Akyaw, K.A., Heckelman, L.N., Cutcliffe, H.C., Sutter, E.G., Englander, Z.A., Spritzer, C.E., Garrett, W.E., DeFrate, L.E., 2017. A comparison of patellofemoral cartilage morphology and deformation in anterior cruciate ligament deficient versus uninjured knees. J. Biomech. 67, 78–83.
- Puxkandl, R., Zizak, I., Paris, O., Keckes, J., Tesch, W., Bernstorff, S., Purslow, P., Fratzl, P., 2002. Viscoelastic properties of collagen: synchrotron radiation investigations and structural model. Philos. Trans. R. Soc. Lond. B Biol. Sci. 357 (1418), 191–197.
- Sampat, S.R., Dermksian, M.V., Oungoulian, S.R., Winchester, R.J., Bulinski, J.C., Ateshian, G.A., Hung, C.T., 2013. Applied osmotic loading for promoting development of engineered cartilage. J. Biomech. 46 (15), 2674–2681.
- development of engineered cartilage. J. Biomech. 46 (15), 2674–2681.

 Setton, L.A., Tohyama, H., Mow, V.C., 1998. Swelling and curling behaviors of articular cartilage. J. Biomech. Eng. 120, 355–361.
- Shanfield, S., Campbell, P., Baumgarten, M., Bloebaum, R., Sarmiento, A., 1988. Synovial fluid osmolality in osteoarthritis and rheumatoid arthritis. Clin. Orthop. Relat. Res. (235), 289–295.
- Shi, L., Sikavitsas, V.I., Striolo, A., 2011. Experimental friction coefficients for bovine cartilage measured with a pin-on-disk tribometer: testing configuration and lubricant effects. Ann. Biomed. Eng. 39 (1), 132–146.
- Soriano-garcia, M., 1976. Balance between swelling pressure and collagen tension in normal and degenerate cartilage growth of algal symbionts in regenerating Hydra. Nature 260, 808–809.
- Sutter, E.G., Widmyer, M.R., Utturkar, G.M., Spritzer, C.E., Garrett, W.E., Defrate, L.E., 2015. In vivo measurement of localized tibiofemoral cartilage strains in response to dynamic activity. Am. J. Sports Med. 43 (2), 370–376.
- Sutter, E.G., Liu, B., Utturkar, G.M., Widmyer, M.R., Spritzer, C.E., Cutcliffe, H.C., Englander, Z.A., Goode, A.P., Garrett, W.E., DeFrate, L.E., 2019. Effects of anterior cruciate ligament deficiency on tibiofemoral cartilage thickness and strains in response to hopping. Am. J. Sports Med. 47 (1), 96–103.
- Tamer, T.M., 2013. Hyaluronan and synovial joint: function, distribution and healing. Interdiscipl. Toxicol. 6 (3), 111–125.
- Urban, J.P.G., Maroudas, A., Bayliss, M.T., Dillon, J., 1979. Swelling pressures of proteoglycans at the concentrations found in cartilaginous tissues. Biorheology 16 (6) 447-464
- Wachtel, E., Maroudas, A., 1998. The effects of PH and ionic strength on intrafibrillar hydration in articular cartilage. Biochim. Biophys. Acta Gen. Subj. 1381 (1), 37–48.
- Wang, P., Fang, J., Qin, S., Kang, Y., Zhu, D.-M., 2009. Moecular weight dependence of viscosity and shear modulus of polyethylene glycol (PEG) solution boundary layers. J. Phys. Chem. 113, 13793–13800.
- Zimmerman, B., Nims, R., Chen, A., Hung, C.T., Ateshian, G.A., 2020. Direct osmotic pressure measurements in articular cartilage demonstrate non-ideal and concentration-dependent phenomena. J. Biomech. Eng.